Journal of Solid State Chemistry 183 (2010) 1496–1503

Contents lists available at ScienceDirect

Journal of Solid State Chemistry

journal homepage: www.elsevier.com/locate/jssc

Synthesis, structure and magnetic properties of V_4O_9—A missing link in binary vanadium oxides

Satoshi Yamazaki [a], Chang Li [a], Kenji Ohoyama [b], Masakazu Nishi [c], Masaki Ichihara [a], Hiroaki Ueda [a], Yutaka Ueda [a,*]

[a] Materials Design and Characterization Laboratory, Institute for Solid State Physics, University of Tokyo, 5-1-5 Kashiwanoha, Kashiwa, Chiba 277-8581, Japan
[b] Institute for Materials Research, Tohoku University, 2-1-1 Katahira, Aoba-ku, Sendai 980-8577, Japan
[c] Neutron Science Laboratory, Institute for Solid State Physics, University of Tokyo, Tokai, Ibaraki 319-1106, Japan

ARTICLE INFO

Article history:
Received 21 December 2009
Received in revised form
7 April 2010
Accepted 8 April 2010
Available online 28 April 2010

Keywords:
V_4O_9
Binary vanadium oxide
Synthesis and crystal structure
Magnetic properties

ABSTRACT

V_4O_9: A missing link of Wadsley phases has been successfully synthesized by using sulfur as a reducing agent at a low temperature and its structure has been determined by combining electron, X-ray and neutron diffractions. V_4O_9 has an orthorhombic *Cmcm* structure and the lattice parameters are $a=10.356(2)$ Å, $b=8.174(1)$ Å and $c=16.559(3)$ Å at room temperature. The structure is composed of shared edges and corners of three types of polyhedra; a VO_6 distorted octahedron, a VO_5 pyramid and a VO_4 tetrahedron. The structure of V_4O_9 is very similar to that of vanadyl pyrophosphate $(VO)_2P_2O_7$ which has PO_4 tetrahedra instead of VO_4 tetrahedra. This indicates that V_4O_9 is a salt of pyro-ion $[V_2O_7]^{4-}$; $(VO)_2V_2O_7$. The magnetic properties of V_4O_9 have been investigated by magnetic susceptibility, high-field magnetization and inelastic neutron scattering measurements. V_4O_9 is a quantum spin system with a spin-gapped ground state. The excitation gap between the singlet ground state and the excited triplet state is approximately 73 K. The magnetic susceptibility behavior suggests that V_4O_9 is a spin-1/2 dimer system with significant interdimer interactions, as opposed to $(VO)_2P_2O_7$, which is an alternating spin-1/2 chain system. This difference is thought to be due to the fact that VO_4-mediated interactions are considerably weaker than PO_4-mediated interactions.

1. Introduction

Binary vanadium oxides have been central target materials in solid state chemistry and physics, because they are very rich not only in the structures but also in physical and chemical properties. Vanadium ions can take various valence states from 2+ to 5+ as in VO, V_2O_3, VO_2 and V_2O_5, respectively. In addition to these monovalent compounds there are many mixed valent compounds represented as V_nO_{2n-1} between V_2O_3 and VO_2 and V_nO_{2n+1} (or $V_{2w}O_{5w-2}$) between VO_2 and V_2O_5, respectively, where n and w are integers. The series compounds V_nO_{2n-1} and V_nO_{2n+1} (or $V_{2w}O_{5w-2}$) have provided good examples of the "shear structure" concept. Furthermore, the binary vanadium oxides have demonstrated various fascinating electromagnetic properties originating from strong electron correlation. The most remarkable properties are metallic conductivity with local moment like magnetic properties and metal–insulator (MI) transition as a function of temperature, which have been a central issue in strongly correlated electron systems [1,2]. With regards to the chemical aspects, V_2O_5 is a well-known catalyst used for the preparation of sulfuric acid from SO_2 with SO_3 formation in the reaction process [3]. To understand the catalytic mechanism, it is important to know the phase relation and metastable phases in the region close to V_2O_5.

The homologous V_nO_{2n-1} series between V_2O_3 and VO_2 are called Magnéli phases [4] and their structures can be understood as the shear structure based on the rutile VO_2 structure [5]. The arrangement of atomic planes parallel to (1 2 1) in the rutile VO_2 structure is [ABAB—], where A=O and B=VO. V_nO_{2n-1} are derived by the shear operations: Periodically eliminate one A-plane every n B-planes and close the resulting gaps by operating a shear vector $1/2[0\,\bar{1}\,\bar{1}]$ (shear planes), consequently obtaining $n\mathrm{VO}+(n-1)\mathrm{O}=V_nO_{2n-1}$. The structures of V_nO_{2n-1} include $n\mathrm{VO}_2$ units between shear planes. Until now, six compounds ($n=3$–8) have been isolated. V_nO_{2n-1} has been extensively studied not only in such structural aspect but also with respect to the electromagnetic properties. Almost all V_nO_{2n-1} compounds ($n=4,5,6,8$) show charge ordered type MI transitions, accompanied by the sharp reduction of the magnetic susceptibility due to the formation of spin-singlet V^{4+}–V^{4+} pairs in the low temperature insulator phases [2]. The unique insulating compound V_3O_5 ($n=3$) among them falls into an antiferromagnetic state

* Corresponding author. Fax: +81 4 7136 3435.
E-mail address: yueda@issp.u-tokyo.ac.jp (Y. Ueda).

0022-4596/$ - see front matter © 2010 Elsevier Inc. All rights reserved.
doi:10.1016/j.jssc.2010.04.007

below T_N=75 K, showing no anomaly at T_N in the magnetic susceptibility curve but the anomalous rotation of the magnetic susceptibility principal axes [6], while the metallic compound V_7O_{13} (n=7) has a rare antiferromagnetic metallic ground state [2].

On the other hand, the homologous V_nO_{2n+1} (or $V_{2w}O_{5w-2}$) series called Wadsley phases have been predicted between VO_2 and V_2O_5 [7], on the basis of the similar "shear structure" concept. However, only two compounds, V_3O_7 (n=3 or w=6) [8,9] and V_6O_{13} (n=6 or w=3) [10], have been obtained in both powder and single crystal forms. The metallic compound V_6O_{13} actually has a structure regarded as a shear structure and shows a MI transition followed by an antiferromagnetic transition in the insulating phase [11,12]. The MI transition is accompanied by a sharp reduction of magnetic susceptibility, which evidences the formation of spin singlet V^{4+}–V^{4+} pairs in the low temperature insulator phase. Whereas the insulating V_3O_7 has a structure constructed from V–O polyhedra with different coordinations; octahedral, bipyramidal and square pyramidal coordinations, and V_3O_7 is a uniaxial antiferromagnet [13,14]. V_nO_{2n+1} (or $V_{2w}O_{5w-2}$) with other n's have been challenged to be synthesized with the expectation of exotic properties such as MI transition. Furthermore, V_nO_{2n+1} (or $V_{2w}O_{5w-2}$) series compounds are important to understand the catalytic mechanism of V_2O_5 in its redox reactions. Particularly, V_4O_9 (n=4 or w=4) with the formal valence of V^{4+}/V^{5+}=1 has been desired to be synthesized. Among V_nO_{2n+1} (or $V_{2w}O_{5w-2}$) series compounds, V_4O_9 has been a special compound in the sense that its structure and properties have remained unclear for a long time although its existence has been recognized widely, namely "a missing link" in binary vanadium oxides. Taniguchi et al., for the first time, confirmed the existence of V_4O_9 from thermogravimetric analysis [15]. Afterward, Wilhelm et al. proposed a crystal structure model of V_4O_9; however, they did not propose detailed atomic positions [16]. Kawashima et al. also predicted the existence of the homologous V_nO_{2n+1} series compounds including V_4O_9 in the process of isothermal reduction of V_2O_5 by SO_2 gas [17]. In addition to these reports there are some reports on V_4O_9 [18], however, neither structure nor properties has been settled yet.

We have strived to synthesize V_4O_9 and to make its structure and properties clear. In this paper, we report successful synthesis of single phase V_4O_9 by a soft chemistry method, the structure determined by using powder sample, and the magnetic properties. Unexpectedly, the solved structure is not a plane fault type (shear structure) but a tunnel defect type. The structure constituted by VO_5 pyramids, VO_6 distorted octahedra and VO_4 tetrahedra is very similar to the structure of vanadyl pyrophosphate $(VO)_2P_2O_7$ with PO_4 tetrahedra instead of VO_4 tetrahedra. This indicates that V_4O_9 is a salt of pyro-ion $[V_2O_7]^{4-}$; $(VO)_2V_2O_7$. V_4O_9 is a low dimensional quantum spin system with a spin-gapped ground state; this is also similar to $(VO)_2P_2O_7$. Although the structure has been determined from only the powder diffraction data because of impossible crystal growth, the resemblance of magnetic properties between V_4O_9 and $(VO)_2P_2O_7$ strongly supports the reliability of the structure.

2. Experimental

Powder samples of V_4O_9 were prepared by a soft chemistry method; the reduction of V_2O_5 by using sulfur at relatively low temperatures. The details are described in the following section. Powder X-ray diffraction (XRD) was measured using a MXP21 Mac Science diffractometer with Cu–$K\alpha$ radiation (λ=1.5405 Å). Thermogravimetric (TG) analysis was carried out using a thermobalance, TG2000S Mac Science analyzer. Transmission electron microscope (TEM) and electron diffraction (ED) were observed using JEOL-EM2010 operated at 200 kV. Powder neutron diffraction (ND) measurements were conducted at room temperature using HERMES (High Efficiency high Resolution MEasurementS) at Institute for Materials Research (IMR), Tohoku University, installed at the JRR-3M reactor in Japan Atomic Energy Research Institute (JAERI), Tokai, Japan. Neutrons with a wavelength of 1.8207 Å obtained by (3 3 1) reflection of the Ge monochromator were used.

The magnetic susceptibility was measured in an external magnetic field of 1.0 T from 2 to 300 K on heating after zero-field cooling with a superconducting quantum interference device (SQUID) magnetometer. The magnetization up to 7 T was measured with a quantum design magnetic property measurement system. The high-field magnetization measurements were performed by a pulsed field magnet at ISSP, University of Tokyo. Inelastic neutron scattering experiments were carried out with the ISSP-PONTA triple axis spectrometer installed at a 5G beam port of JRR-3M at the Japan Atomic Energy Institute. A powder sample of 30.0 g was put into an aluminum cylinder. Most of data were collected using a fixed final energy E_f of 8.0 meV (k_f=2.67) and a horizontal collimation of open-40-S-40-80 in combination with a pyrolytic graphite (PG) filter placed after the sample to eliminate high-order beam contaminations. This setup yields an energy resolution of 1.21 meV at Q=1.2 Å^{-1} and E=0, as determined by measuring the incoherent scattering from the sample.

3. Results

3.1. Synthesis

V_4O_9 has been impossible to be synthesized by a solid state reaction of an appropriate mixture with binary V_2O_5 and V_2O_3 (or VO_2). The previous studies employed the reduction of V_2O_5 using reducing agents of carbon, SO_2, etc. or under ultra high vacuum. Until now, however, there has been no report which describes successful synthesis of single phase V_4O_9. After much trial and error, we found the best method by using sulfur as a reducing agent.

The synthesis was conducted as follows: V_2O_5 and S with an appropriate ratio was mixed, ground thoroughly and pressed into a pellet. The pellet was sealed into an evacuated silica tube and heated at 400 °C for 1 day. The reaction is represented as

$$4V_2O_5+S \rightarrow 2V_4O_9+SO_2$$

Since XRD pattern of V_4O_9 has not been established, it is difficult to identify V_4O_9 from XRD pattern. However, a systematic change of XRD pattern of the product in varying the ratio of V_2O_5 and S made the phase identification possible. As shown in Fig. 1(a), the stoichiometric ratio (V_2O_5/S=4) always gave the second phase of VO_2(B), which could be because oxygen of V_4O_9 was further removed by produced SO_2 gas, according to the reaction as

$$SO_2+1/2O_2 \leftrightarrow SO_3$$

By further increasing the amount of S, the VO_2(B) phase was increased in quantity. Then the amount of S was decreased. In the reaction with less than 92% of S to the stoichiometric ratio, a part of V_2O_5 remained unreduced, as shown in Fig. 1(c). In the case of 92–94% of S, the XRD pattern indicated the absence of any known impurity phases including V–O binary and V–S–O ternary systems, as shown in Fig. 1(b). Then the obtained XRD pattern can be assigned to that of V_4O_9. A similar XRD pattern was previously reported [17,18], although it was not identified as that of V_4O_9.

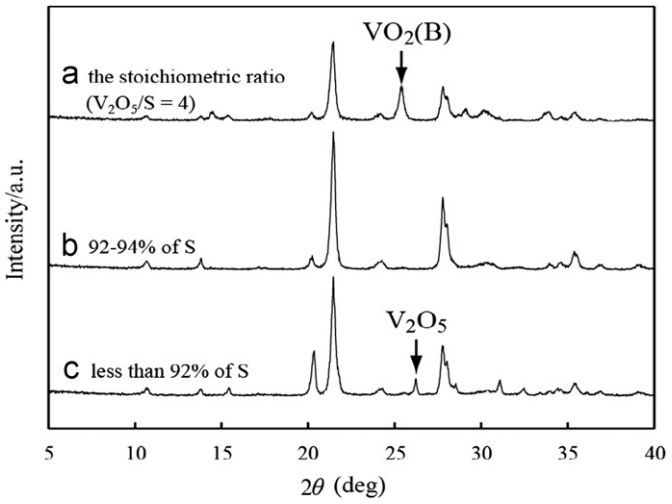

Fig. 1. X-ray diffraction profiles of the samples synthesized with (a) the stoichiometric ratio of V_2O_5 and S, (b) 92–96% of S and (c) less than 92% of S to the stoichiometric ratio, at 400 °C for 1 day. At the stoichiometric ratio of V_2O_5/S=4, the product always includes VO_2(B), while at less than 92% of S, a part of V_2O_5 remains unreduced.

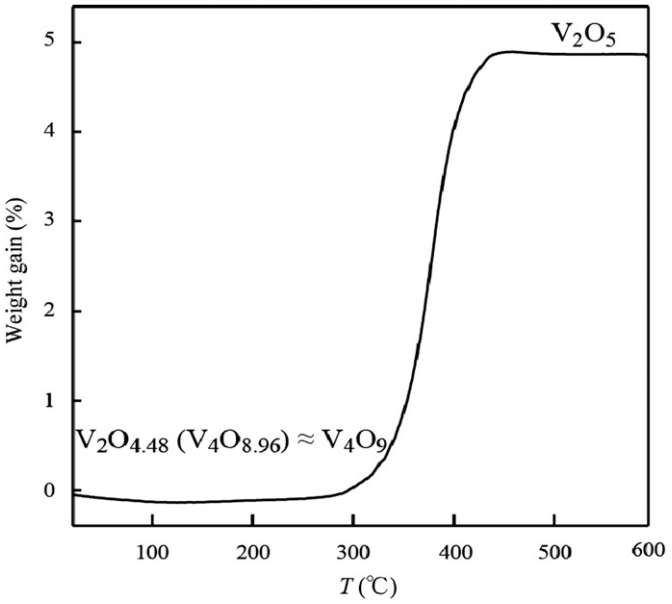

Fig. 2. Thermogravimetric curve measured under oxygen gas flow. The composition calculated from the weight gain is $V_2O_{4.48}$ close to V_4O_9.

To confirm the composition of oxygen, we measured TG up to 600 °C in O_2 gas flow; under O_2 gas atmosphere, the starting substance would be oxidized to V_2O_5. The weight began to increase above 300 °C and saturated at around 4.8% above 450 °C, as shown in Fig. 2. The oxidized product was surely identified to be V_2O_5 from XRD. From this weight gain, the original composition was determined to be $VO_{2.24}$, namely $V_4O_{8.96}$, which was in good agreement with the composition V_4O_9 within experimental error. It should be emphasized that this method using S has advantages; easy handling of the reagents and production of a large amount of samples.

3.2. Crystal structure

Since the synthesis method and temperature are limited, it is impossible to grow single crystals of V_4O_9. We have challenged to solve the crystal structure by using powder samples, combining ED, XRD and ND. We first constructed the reciprocal lattice and then determined lattice parameters from ED in TEM observation, because the object was a single crystal in the scope of TEM observation. The ED pattern shown in Fig. 3(a) was observed most frequently and easily. This suggests that V_4O_9 has a layer structure with a cleavage plane perpendicular to zone axis of this ED pattern. By rotating the same crystal around the axis indicated by a broken line in Fig. 3(a), we obtained another ED pattern shown in Fig. 3(b). By combining these ED patterns, the three dimensional reciprocal lattice can be built, as shown in Fig. 3(c). From this reciprocal lattice, the crystal system is an orthorhombic one with a C-centered lattice where the directions of *a*-, *b*-, and *c*-axis are taken as shown in Fig. 3(c). Here, note that the pattern in Fig. 3(a) corresponds to the *ab*-plane. The lattice parameters are roughly calculated to be $a=10.3$ Å, $b=8.2$ Å and $c=16.6$ Å.

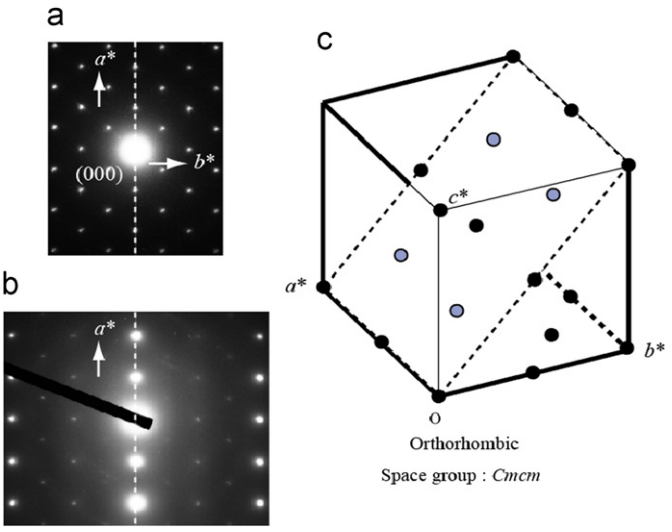

Fig. 3. Electron diffraction (ED) patterns of V_4O_9. (a) The most frequently and easily observed ED pattern corresponding to the hypothetical *ab*-plane. (b) ED pattern obtained by rotating the same crystal around the broken line in (a). (c) The three dimensional reciprocal lattice built by combining these ED patterns.

Using the obtained lattice parameters as starting values, XRD pattern was well-fitted by Le Bail analysis. This analysis gave us indices of peaks in XRD and ND patterns with the refined lattice parameters; $a=10.356(2)$ Å, $b=8.174(1)$ Å and $c=16.559(3)$ Å. Comparing these indices with the extinction rule, a possible space group was determined as follows: There are 24 candidates of space groups with an orthorhombic and C-centered lattice. First, we checked for the existence of glide planes. For example, to have *c*-glide planes in (1 0 0), 0kl reflections must satisfy $k+l=2n$. The observation of 021 peak in XRD and ND indicates the absence of *c*-glide plane. Since *a*- and *b*-glide planes are absent as well, possible space groups are restricted to nine candidates, *C*222, *C*2*mm*, *Cm*2*m*, *Cmm*2, *Cmmm*, $C222_1$, *C*2*cm*, $Cmc2_1$ and *Cmcm*, namely *Cmmm*, *Cmcm* and their subgroups. Among them, *C*222, *Cmm*2, *Cm*2*m*, *C*2*mm* and *Cmmm* are ruled out from the result that 001 peak is not observed in XRD and ND patterns. The remaining four space groups; $C222_1$, *C*2*cm*, $Cmc2_1$ and *Cmcm*, are subgroups of *Cmcm*, and therefore *Cmcm* is the most symmetrical one. We take *Cmcm* as the most likely candidate.

To determine unknown structure from powder diffraction data, it is very useful and necessary to construct a plausible structural model. A hint for a model is in the synthesis process. V_4O_9 is obtained by reducing V_2O_5 with S at relatively low temperatures and further reduction produces VO_2(B). This suggests that V_4O_9 has a modified structure from those of V_2O_5

and/or VO_2(B). The crystal structures of V_2O_5 and VO_2(B) are shown in Fig. 4. The layered structure of V_2O_5 is built from highly distorted VO_6 octahedra, sharing their edges and corners. In the *ab*-plane, VO_6 octahedra form edge-sharing zig-zag chains running along the *b*-axis and these zig-zag chains are joined together by sharing of the corner oxygen atoms to form so-called trellis lattice. Thus formed trellis lattice layers (α-layers) are stacked, sharing oxygen atoms (β-layers) on the corner with a distance *c* apart. Hence, the structure of V_2O_5 has the stacking of layers as [αβα—] in the *c*-direction or parallel to the *ab*-plane, where the compositions of α- and β-layers are V_2O_3 and O_2, respectively. The interlayer chemical bond is so weak that the crystal is easily cleaved parallel to the *ab*-plane. On the other hand, the crystal structure of VO_2(B), which has the [αβααβαα—] stacking, can be regarded as a daughter structure of V_2O_5 in the "shear structure" concept [19]. The stacking manner of [αβααβαα—] is obtained from V_2O_5 by the shear operations: Periodically eliminate one β-layer every two α-layers as the arrangement of [αβα□αβα□α—] (□: gap) and close the gaps by connecting each [αβα]-block with the shared-edges, obtaining the stacking manner of [αβααβαα—] as shown in Fig. 4. It should be noted that VO_2(B) keeps the trellis lattice structure (double trellis lattice;αα).

Hence, it is reasonable to suppose that V_4O_9 would have a stacking structure of trellis lattices with a cleavage plane. Actually, the ED pattern shown in Fig. 3(a) is often observed in TEM without any tilting operation. This suggests that the *ab*-plane of V_4O_9 is a cleavage plane with a trellis lattice similar to that of V_2O_5 or VO_2(B). If the structure of V_4O_9 were a "shear structure" derived from V_2O_5, it would have a stacking manner of [αβαβαβααβαβαβα—]. This stacking manner is derived by two operations; periodic elimination of one β-layer every four α-layers (αβαβαβα□αβαβαβα□—) and closing the gaps, consequently obtaining the composition of V_4O_9 ($8V_2O_3+6O_2=4V_4O_9$). However, the observed *c*-parameter of 16.6 Å is much shorter than the calculated value of 27.9 Å for the stacking periodicity of [αβαβαβααβαβαβα] (six αβα blocks and one αα block), assuming the thicknesses of 4.34 Å for the αβα block and 1.90 Å for αα block, respectively, from the lattice parameters of V_2O_5 and VO_2(B). The value of 16.6 Å is rather than close to the thickness of four αβα blocks; the stacking periodicity of [αβαβαβαβα]. To obtain the composition of V_4O_9, however, half of oxygen atoms should be removed from half of β-layers in this stacking periodicity. A possible model is shown in Fig. 4. This model has a stacking periodicity of [αβαβ′αβαβ′α] in which half of oxygen atoms in β′-layers are deficient in an ordered manner to form tunnel defects. Hence, the composition is $4V_2O_3$ (α-layers)+$2O_2$ (β-layers) +2O (β′-layers)=$2V_4O_9$.

Taking this structural model in mind, we have to consider atomic positions to solve the crystal structure of V_4O_9. Suppose the density of V_4O_9 and V_2O_5 are almost the same, the Z value of V_4O_9 is estimated to be eight. Then, V_4O_9 has 32 vanadium atoms and 72 oxygen atoms in the unit cell. These atoms should be assigned to Wyckoff positions. The candidate space group (*Cmcm*) has eight Wyckoff positions. At first, we determined Wyckoff positions of vanadium atoms as follows: There are four V–O layers (α-layers) and four oxygen layers (β- and β′-layers) parallel to the *ab*-plane in the unit dell of the structural model mentioned above. The space group (*Cmcm*) has two mirrors at $z=1/4$ and $z=3/4$. These mirrors should be located on V–O layers or oxygen layers and the origin is on a V–O layer or an oxygen layer, respectively. In the case of V–O layers, the vanadium sites on the mirror are 8*g* or 4*c* and those on $z\sim0$ are 8*f* or 16*h*. There are nine combinations of Wyckoff position assignment in this case. In the other case of oxygen layers, the vanadium sites are 8*f* and 16*h* and the combinations are limited to three. Then, total possible combinations of Wyckoff positions are summed up to 12 candidates.

To determine the position of vanadium atoms, we calculated XRD pattern and compared it with XRD data. Placing vanadium atoms at the sites obtained from above-mentioned possible combinations of Wyckoff positions without oxygen atoms, we conducted more than three hundreds million simulations as a first step. We selected proper candidates which satisfied the condition that the simulated intensities of 30 reflections were within the range of 1/2 to 2 times as large as the experimental values. Furthermore, some candidates with too close distances (less than 2 Å) between two vanadium atoms were removed from the selected candidates. As a result, we obtained about 300 likely candidates for vanadium coordination. They have vanadium atoms at three sites, 16*h*, 8*f* and 8*f*, and the mirrors on oxygen layers. Subsequently, possible positions of oxygen atoms were considered. To restrict possible candidates of oxygen positions, we used the conditions that the interatomic distance between vanadium and oxygen should be between 1.6 and 2.6 Å [20] and that half of oxygen atoms should be removed from every two oxygen layers. For each remaining candidate of vanadium positions, we added oxygen atoms at the positions which satisfied these conditions. Finally, we performed XRD simulations with both vanadium and oxygen atoms at possible vanadium and oxygen positions. In the simulations, only 25 candidates with VO_4 tetrahedra gave consistent XRD patterns. Among them, we adopt one candidate that has the most regular VO_4 tetrahedra, because VO_4 tetrahedra in all of vanadium oxides are almost regular [20].

The atomic positions in this candidate were refined by Rietveld analyses of XRD and ND data [21]. The results are shown in Fig. 5 and the refined atomic positions are listed in Table 1.

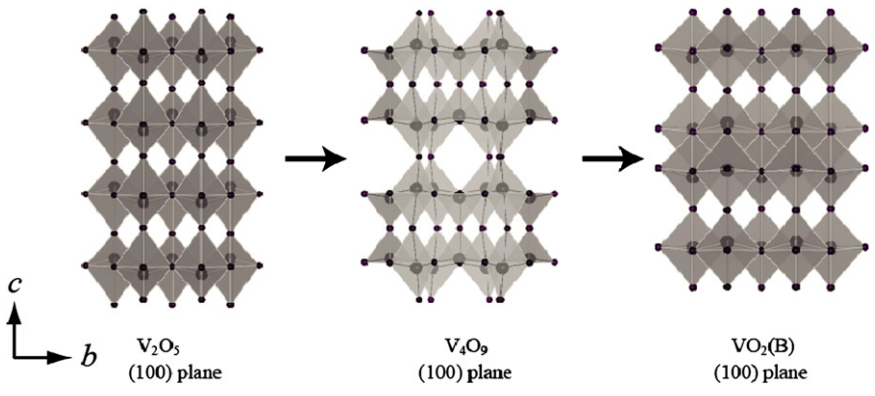

Fig. 4. A structural model of V_4O_9 and the structural relation among V_2O_5, V_4O_9 and VO_2(B). The structures of V_2O_5, V_4O_9 and VO_2(B) are schematically represented by V–O polyhedra. The structure of VO_2(B) is derived from V_2O_5 by the shear operations (see the text).

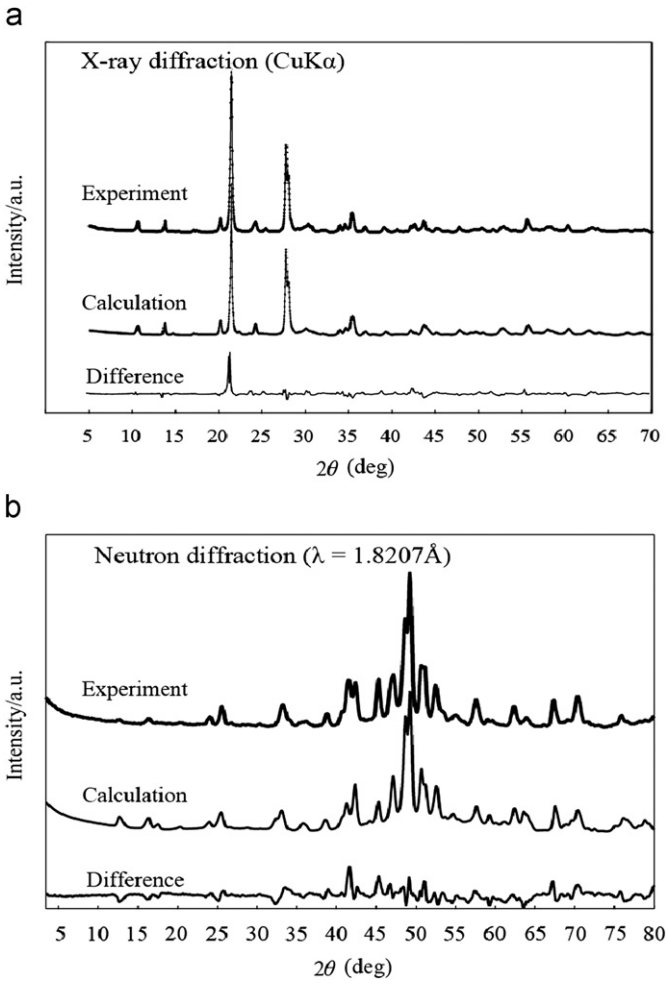

Fig. 5. Rietveld analyses of (a) X-ray diffraction (XRD) and (b) neutron diffraction (ND) patterns of V_4O_9 in the space group of *Cmcm*. The *R*wp-value is 13.2% for XRD and 14.3% for ND.

Table 1
Atomic positions and atomic displacement parameters for V_4O_9. Space group *Cmcm*; $a=10.356(2)$ Å, $b=8.174(1)$ Å, $c=16.559(3)$ Å; Z=8: Atomic parameters of V atom were refined using XRD data (*R*wp=13.2%), while those for O atom were done using ND data (*R*wp=14.3%).

Atom	Site	*x*	*y*	*z*
V(1)	8*f*	0.500	0.205(0)	0.156(7)
V(2)	8*f*	0.000	0.353(4)	0.130(3)
V(3)	16*h*	0.209(4)	0.013(2)	0.096(0)
O(1)	4*c*	0.000	0.320(3)	0.250
O(2)	4*c*	0.500	0.209(7)	0.250
O(3)	8*e*	0.204(6)	0.000	0.000
O(4)	8*f*	0.000	0.338(9)	0.001(0)
O(5)	16*h*	0.371(0)	0.002(0)	0.132(9)
O(6)	16*h*	0.138(4)	0.191(3)	0.120(4)
O(7)	16*h*	0.366(2)	0.318(7)	0.130(5)

The *R*wp-value is about 13% which is somewhat large. Such a large *R*wp-value is partly due to crystal orientation and is mainly due to relatively broad diffraction peaks which originate from poor crystallinity of the sample. Such poor crystallinity is inevitable in the sample synthesized by the reduction method at relatively low temperatures. Actually, the *R*wp was reduced to 11% by adjusting an orientation parameter and TEM observation revealed fine particles and poor crystallinity of the sample. We did not perform further refinement with space groups of lower symmetry, because the obtained structure included various aspects which convinced the reliability, as described below. Our aim is to determine the structure of this new compound at necessary and enough level to understand its chemical and physical properties, under the situation that its single crystals could be hard to be synthesized at present and even in future.

The crystal structure of V_4O_9 is shown in Fig. 6. The structure belongs to an orthorhombic *Cmcm* structure and the lattice parameters are $a=10.356(2)$ Å, $b=8.174(1)$ Å and $c=16.559(3)$ Å at room temperature. In this structure, there are three vanadium sites and seven oxygen sites. The V(1) site has a pyramidal coordination of oxygen; one apical oxygen atom of the distorted $V(1)O_6$ octahedra is far from the V(1) site along the *c*-direction. We call this as $V(1)O_5$ pyramid. On the other hand, the V(2) site has a oxygen-coordination close to octahedral; $V(2)O_6$ octahedron. The V(3) site has a tetrahedral coordination of oxygen; $V(3)O_4$ tetrahedron. The interatomic distances and bond angles in these polyhedra are listed in Table 2. In the *ab*-plane of this structure, $V(1)O_5$ pyramids and $V(2)O_6$ octahedra make pairs with shared edges and these pairs are bridged by $V(3)O_4$ tetrahedra. The *ab*-plane in Fig. 6 represents thus formed layer which corresponds to α-layer of the model in Fig. 4. To form the three dimensional structure, the layers form a double layer with shared corners of these polyhedra as $V(1)O_5$ pyramids–$V(2)O_6$ octahedra and $V(3)O_4$–$V(3)O_4$ tetrahedra along the *c*-axis and thus formed double layers are joined by sharing of the corner oxygen atoms of $V(1)O_5$ pyramids and $V(2)O_6$ octahedra, respectively, as shown in Fig. 6, obtaining the stacking manner like [αβαβ′αβαβ′α—]. Consequently, the pairs of the edge-shared $V(1)O_5$ and $V(2)O_6$ form two-leg ladder chains along the *c*-axis and alternating chains along the *b*-axis, and $V(3)O_4$ tetrahedra bridge the ladder chains or the pairs. According to the literature on vanadium oxides [20], the valence of vanadium ion in a distorted octahedron and a pyramid is +4 or +5, and that in a tetrahedron is definitely +5. Since the ratio of V(1):V(2):V(3) is 1:1:2 in this structure, the valences of vanadium ions in V_4O_9 are clearly assigned to +4 for the V(1) and V(2) sites and +5 for the V(3) sites.

The obtained structure of V_4O_9 is very similar to that of vanadyl pyrophosphate $(VO)_2P_2O_7$ which is a salt of pyro-ion $[P_2O_7]^{4-}$. There exist two morphologies of $(VO)_2P_2O_7$; the ambient pressure phase, AP-$(VO)_2P_2O_7$ [22] and the high pressure phase, HP-$(VO)_2P_2O_7$ [23]. The crystal structures of both phases

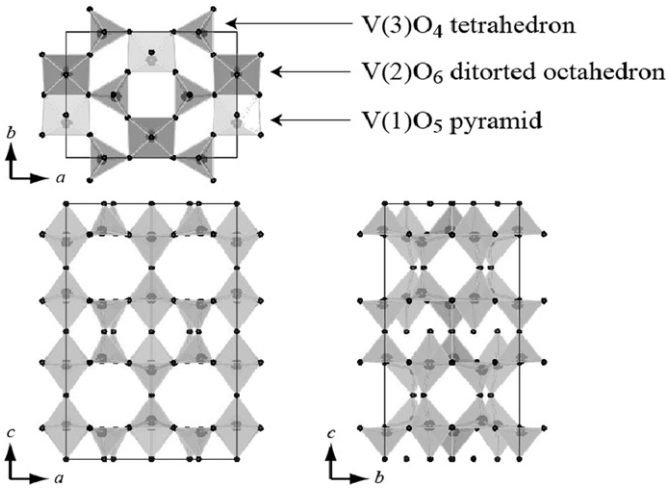

Fig. 6. The crystal structure of V_4O_9 viewed along the *c*-, *b*- and *a*-axis of an orthorhombic *Cmcm* structure. It consists of three types of V–O polyhedra, $V(1)O_5$ pyramid, $V(2)O_6$ octahedron and $V(3)O_4$ tetrahedron (see the text).

Table 2
Bond distances (Å) and bond angles (deg.) for V_4O_9. There are three vanadium sites, V(1)–V(3) and seven oxygen sites, O(1)–O(7), in the structure.

V–O polyhedra	Diatances (Å)		Angles (deg.)	
V–O octahedron	V(2)–O(1)	2.001	O(1)–V(2)–O(4)	170.0
	V(2)–O(4)	2.107	O(1)–V(2)–O(5)	93.8
	V(2)–O(5)	1.810	O(1)–V(2)–O(6)	89.4
	V(2)–O(6)	1.962	O(5)–V(2)–O(4)	93.4
			O(5)–V(2)–O(5)	95.4
			O(5)–V(2)–O(6)	85.1
			O(6)–V(2)–O(4)	83.1
			O(6)–V(2)–O(6)	94.2
V–O pyramid	V(1)–O(2)	1.646	O(2)–V(1)–O(5)	99.0
	V(1)–O(5)	2.167	O(2)–V(1)–O(7)	103.7
	V(1)–O(7)	1.725	O(5)–V(1)–O(5)	76.8
			O(5)–V(1)–O(7)	82.6
			O(7)–V(1)–O(7)	106.9
V–O tetrahedron	V(3)–O(3)	1.621	O(3)–V(3)–O(5)	111.0
	V(3)–O(5)	1.778	O(3)–V(3)–O(6)	106.1
	V(3)–O(6)	1.676	O(3)–V(3)–O(7)	103.6
	V(3)–O(7)	1.863	O(5)–V(3)–O(6)	112.1
			O(5)–V(3)–O(7)	104.1
			O(6)–V(3)–O(7)	118.8

consist of two types of polyhedra; VO_5 pyramids (or distorted VO_6 octahedra) and PO_4 tetrahedra. The pairs of the edge-shared VO_5 pyramids form two-leg ladder chains and PO_4 tetrahedra bridge the ladder chains or the pairs. This manner is very similar to that in the obtained structure of V_4O_9, although VO_4 tetrahedra instead of PO_4 bridge the two-leg ladder chains or the pairs in V_4O_9. Therefore, V_4O_9 can be represented as $(VO)_2V_2O_7$ which is obtained by replacing PO_4 tetrahedra in $(VO)_2P_2O_7$ with VO_4 tetrahedra. Actually, the expression of $(VO)_2V_2O_7$ is better rather than V_4O_9 as the chemical formula, because V_4O_9 can be regarded as a salt of pyro-$[V_2O_7]^{4-}$ ion, namely vanadyl pyrovanadate. In general, pentavalent V^{5+} behaves like P^{5+} in forming the ions $[VO_4]^{3-}$ and $[V_2O_7]^{4-}$ similar to the ions $[PO_4]^{3-}$ and $[P_2O_7]^{4-}$. There are many salts of the pyro-ions $[V_2O_7]^{4-}$ and $[P_2O_7]^{4-}$, which are isostructural. Such similarities between V_4O_9 and $(VO)_2P_2O_7$ convince us that the obtained structure of V_4O_9 is reliable. V_4O_9 shows similar magnetic properties to $(VO)_2P_2O_7$, as described below. This also supports the reliability of the obtained structure.

3.3. Magnetic properties

Fig. 7 shows the temperature (T) dependence of magnetic susceptibility (χ) measured by using the obtained V_4O_9 powder samples. The raw data of magnetic susceptibility (χ_{raw}) shows a broad maximum centered around 70 K. When the temperature is further decreased, χ_{raw} shows a rather sharp decrease and finally shows a sharp increase below 15 K. χ_{raw} can be fitted to the following equation: $\chi_{raw}=\chi_{spin}+\chi_0+\chi_{imp}$, where χ_{spin} is the intrinsic d-spin susceptibility of V_4O_9; χ_0, a temperature-independent constant term; and χ_{imp}, the contribution of free spins due to impurities or defects. χ_{imp} is responsible for the sharp increase in χ_{raw} below 15 K. This increase obeys a Curie law expressed as C/T, where C is a Curie constant. The best fit gives $\chi_0=3.4\times10^{-4}$ emu/V-mol and $C=5.47\times10^{-3}$ emu/V-mol. The obtained value of C corresponds to an impurity concentration of approximately 1.5%, assuming a spin-1/2. The solid line in Fig. 7 shows χ_{spin} obtained by subtracting $(\chi_0+\chi_{imp})$ from χ_{raw}. χ_{spin} shows a broad maximum at around 80 K and then decreases to almost zero as the temperature decreases below 15 K. Similar behaviors are observed in one-dimensional (1D) magnets with a spin-gapped ground state, for examples, alternating chain and two-leg ladder chain systems. To estimate the gap energy, χ_{spin} below 30 K is fitted to the equation; $\chi_{spin}=aT^{-1/2}\exp(-\Delta/T)$, which indicates the susceptibility of a 1D system with a spin gap of Δ [24], as shown by the dotted line in Fig. 7. The best fit gives $a=6.0\times10^{-2}$ and $\Delta=72$ K.

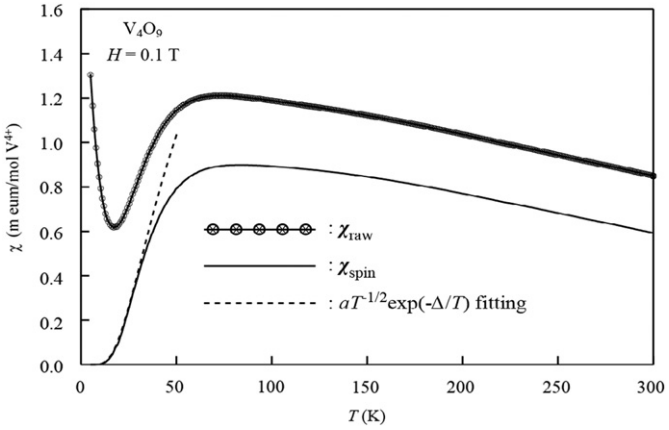

Fig. 7. Temperature dependence of magnetic susceptibility (χ_{raw}) of V_4O_9 measured at 0.1 T. The intrinsic d-spin susceptibility (χ_{spin}) of V_4O_9 after subtracting the Curie tail and the temperature independent term is shown by the solid line (see the text). The dotted line shows a fitting to the equation: $\chi_{spin}(T)=aT^{-1/2}\exp(-\Delta/T)$ for a one-dimensional (1D) magnet with a spin gap of Δ (see the text).

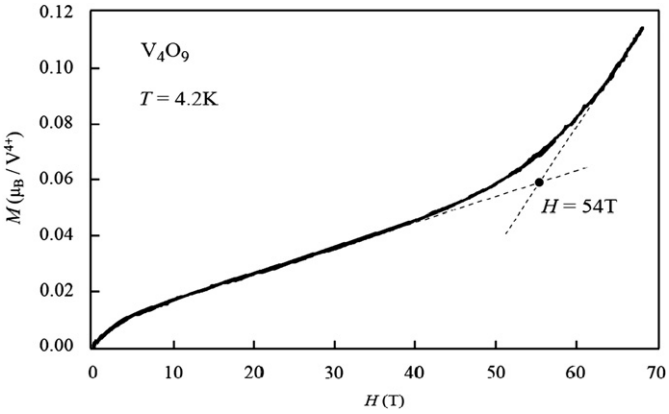

Fig. 8. Magnetization curve of V_4O_9 up to 70 T measured by a pulsed field magnet at 4.2 K. The level crossing between the singlet ground state and the excited triplet state occurs around the critical field of $H_c\sim54$ T.

Next we measured the high-field magnetization (M) to observe the field-induced transition to a gapless state in high fields. The obtained result is shown in Fig. 8. Under relatively low fields, the magnetization curve tends to saturate because of the presence of free spins from impurities or defects. With a further increase in the applied field, the magnetization linearly increases up to around 40 T. Above 60 T, it increases more steeply, indicating that the level crossing between the singlet ground state and the excited triplet state occurs at around the critical field H_c ($\sim$54 T). The excitation gap can be expressed as $\Delta(H)=\Delta-g\mu_BH$, where Δ is the excitation gap at zero field. From the H_c value, Δ/k_B can be estimated to be approximately 73 K, which is in good agreement with the Δ value ($\sim$72 K) obtained from the analysis of χ_{spin}. The linear component in the magnetization curve below 40 T can be attributed to the orbital susceptibility (Van Vleck term), because the magnetic susceptibility obtained from the slope (5.16×10^{-4} emu/V-mol) is close to χ_0.

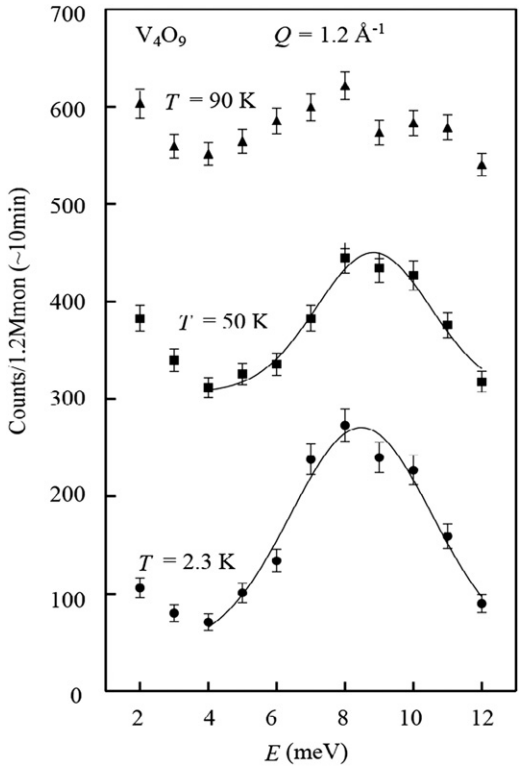

Fig. 9. Inelastic neutron scattering spectra at $Q=1.2\,\text{Å}^{-1}$ for V_4O_9. An excitation peak around 8 meV is observed below 80 K, indicating that V_4O_9 falls into a spin-gapped ground state below 80 K.

The spin-gapped ground state was also confirmed from inelastic neutron scattering experiments. The obtained spectra are shown in Fig. 9. Below 70 K, an excitation peak can be clearly observed at around 8 meV, which is approximately equal to the gap energy of 73 K determined from high-field magnetization experiments.

4. Discussion

Now V_4O_9 is unveiled. The structure of V_4O_9 cannot be explained on the basis of the "shear structure" concept. It should be noted that the essential feature of a "shear structure" is the presence of oxygen-plane-faults (shear plane). The obtained structure can be regarded as an ordered structure with oxygen-point-defects (tunnel defects), similar to the structure of Brown-millerite family. This explains why further reduction of V_4O_9 affords VO_2(B) instead of V_6O_{13}. VO_2(B) is easily obtained from V_4O_9 by the elimination of the residual oxygen atoms present in the same plane. On the other hand, the structure of V_6O_{13} is considerably different from that of V_4O_9, and hence, to obtain V_6O_{13}, the atoms in V_4O_9 must be drastically rearranged. In a certain sense, the structure of V_4O_9 is intermediate between that of V_2O_5 and VO_2(B). To the best of our knowledge, this is the first observation of such an intermediate compound in shear-structure systems.

V_4O_9 is thought to play an important role in catalytic reactions involving V_2O_5. V_2O_5 is a well-known catalyst used for the preparation of sulfuric acid from SO_2; in this process, SO_3 is also formed. However, the details of the catalytic reaction including the intermediate states have not been clarified. SO_3 is formed when V_4O_9 is synthesized from V_2O_5 and S (SO_2). This fact suggests a strong possibility of V_4O_9 being temporarily formed on the surface of V_2O_5 during the course of the catalytic reaction. Furthermore, V_4O_9 itself may act as a catalyst because its structure is similar to that of $(VO)_2P_2O_7$, which is a well-known catalyst, as is V_2O_5 [25]. Hence, the catalytic reaction may be investigated on the basis of the structure of V_4O_9.

V_4O_9 is a spin-1/2 1D antiferromagnetic quantum spin system with a spin-gapped ground state. The structure and magnetic properties of V_4O_9 are similar to those of AP- and HP-$(VO)_2P_2O_7$. AP-$(VO)_2P_2O_7$ has a distorted monoclinic structure with a space group of $P2_1$ [26]; on the other hand, HP-$(VO)_2P_2O_7$ has a simple orthorhombic structure with a space group of Pnab [27]. Both $(VO)_2P_2O_7$ and V_4O_9 have similar basic structures; in $(VO)_2P_2O_7$ and V_4O_9, spin-1/2 V^{4+} ions are bridged by $P^{5+}O_4$ and $V^{5+}O_4$, respectively, as shown schematically in Fig. 10. In this figure, the *a*-, *b*- and *c*-axes in the structure of $(VO)_2P_2O_7$ correspond to the *c*-, *a*- and *b*-axes in the structure of V_4O_9 (Fig. 6), respectively. It is apparent that in these two compounds, the V^{4+} ions form alternating chains (the solid line) in the *c*-direction or two-leg ladder chains (the dotted line) in the *a*-direction. In early stage, AP-$(VO)_2P_2O_7$ was considered as a spin ladder system ($J_\perp$ and J_2 in Fig. 10) [22]. Recently, however, it was confirmed that AP-$(VO)_2P_2O_7$ is a spin-1/2 alternating chain system (J_1 and J_2 in Fig. 10). In AP-$(VO)_2P_2O_7$, there exist two types of alternating chains (chain A and chain B) with two different gaps ($\Delta/k_B=35$ K and 68 K for chains A and B, respectively) [28,29]. The magnetic interactions in each alternating chain include the interdimer interaction (J_1) along the V–O–P–O–V path and the intradimer interaction (J_2) along the V–O–V path. The dominant magnetic interaction is J_1 mediated by the PO_4 tetrahedra that bridge the magnetic V^{4+} dimers. It is found that J_1 is stronger than J_2: $J_1=136$ K, $J_2=92$ K, and α ($=J_2/J_1$)$=0.67$ for chain A, while $J_1=124$ K, $J_2=103$ K, and $\alpha=0.83$ for chain B [29]. On the other hand, in HP-$(VO)_2P_2O_7$, which has a simple orthorhombic structure, only one type of alternate chain is present; in this case, $\alpha=0.87$ ($J_1=132$ K and $J_2=115$ K) and $\Delta/k_B\sim33$ K [27]. The parameters J_1 and J_2 for these two phosphates were obtained by the analytical fitting of $\chi(T)$ on the basis of the theoretical prediction of $\chi(T, J_1, J_2)$ for a spin-1/2 antiferromagnetic alternating-exchange (J_1, J_2) Heisenberg chain [30,31]. According to this theoretical prediction, all the $\chi(T, J_1, J_2)$ curves show rounded maxima, which is characteristic of 1D systems, at finite temperatures. Further, when α varies from the dimer limit ($\alpha=0$) to the uniform limit ($\alpha=1$), the value of susceptibility maximum (χ_{max}) is significantly reduced, while the temperature of maximum susceptibility (T_{max}) shows no notable change. The gap energy also decreases with increasing α from $\Delta/|J|=1$ at $\alpha=0$ (isolated dimer) to $\Delta/|J|=0$ at $\alpha=1$ (1D uniform chain). According to the theoretical prediction, the degree of alternation can be estimated as follows: Determine J_1 from the relation $kT_{max}/J_1\approx1.25$, and convert χ_{max} to reduced unit $J_1\chi_{max}/Ng^2\mu_B^2$; then

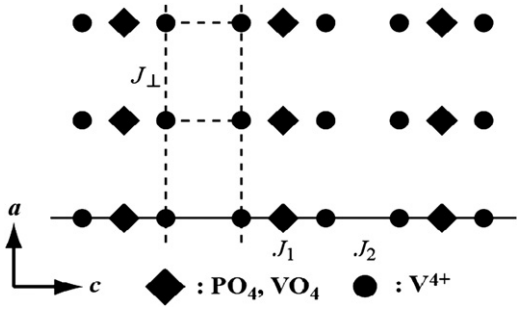

Fig. 10. Sketch of the basic structure formed by spin-1/2 V^{4+} ions in V_4O_9 and $(VO)_2P_2O_7$. The V^{4+} ions form an alternating chain (the solid line) with exchange constants J_1 and J_2 along the *c*-axis and a two-leg ladder chain (the dotted line) with exchange constants $J_\perp$ and J_2 along the *a*-axis.

obtain the value of α from the figure provided in the literature [30]. By using the T_{max} (80 K) and χ_{max} (1.1×10^{-3} emu/V-mole) values for V_4O_9, we calculate $J_1\chi_{max}/Ng^2\mu_B^2$ to be approximately 0.053. This value is considerably smaller than that ($\sim$0.073) for the uniform limit ($\alpha=1$). This implies that V_4O_9 is not an alternating chain system. Comparison of the susceptibility behavior of V_4O_9 with that of alternating chain systems reveals that above T_{max}, χ_{spin} of V_4O_9 is very small, indicating the weak temperature dependence of magnetic susceptibility. Such a behavior has been observed in spin-1/2 ladder systems [32] and orthogonal dimer systems [33] with strong interdimer coupling. These results indicate that the J_1 mediated by VO_4 is considerably weaker than the intradimer coupling (J_2) or even negligible. It is noteworthy that CsV_2O_5, in which the V_2O_5 layer has a similar structure to that of the *ab*-plane in V_4O_9 (Fig. 6), is a typical isolated dimer system; this indicates that VO_4-mediated interaction is negligible [32]. Therefore, the fundamental magnetic unit in V_4O_9 would be the dimers formed by edge-sharing $V(1)O_6$ and $V(2)O_6$. The dimers form a two-leg ladder with alternating distances between dimers (rungs) along the *c*-axis, as shown in Fig. 6; this structure is different from that of the two-leg ladder with equal distance between dimers (rungs) in AP- or HP-$(VO)_2P_2O_7$. The alternating distances in V_4O_9 originate from the VO_4 tetrahedra (pyro-ions $[V_2O_7]^{4-}$) pairs formed by sharing of the corner oxygen atoms along the *c*-axis, as shown in Fig. 6. At present, it is impossible to analyze $\chi_{spin}(T)$ from such alternating spin-ladder model or coupled dimer model because of the lack of theoretical predictions for these models. The observed similarity and difference between the magnetic properties of V_4O_9 and $(VO)_2P_2O_7$ are in good agreement with the similarity and difference between the structures of these compounds. This further supports the accuracy of the obtained structure of V_4O_9.

5. Summary

V_4O_9: A "missing link" of Wadsley phases between VO_2 and V_2O_5 has been successfully synthesized by a soft chemistry method using sulfur as a reducing agent at a low temperature. The structure of V_4O_9 has been determined by a combination of electron, X-ray and neutron diffraction analyses. The most plausible structure of V_4O_9 is an orthorhombic *Cmcm* structure, and the lattice parameters are $a=10.356(2)$ Å, $b=8.174(1)$ Å and $c=16.559(3)$ Å at room temperature. This structure is composed of the shared edges and corners of three types of polyhedra; a distorted $V(1)O_6$ octahedron, a $V(2)O_5$ pyramid and a $V(3)O_4$ tetrahedron, where the valence state is +4 for the V(1) and V(2) sites and +5 for the V(3) sites and the V(1):V(2):V(3) ratio is 1:1:2. Thus, the chemical formula of V_4O_9 is represented as $(V^{4+}O)_2V_2^{5+}O_7$, which indicates that V_4O_9 is a pyrovanadate. The structure of V_4O_9 is very similar to that of vanadyl pyrophosphate $(V^{4+}O)_2P_2^{5+}O_7$ which has PO_4 tetrahedra instead of VO_4 tetrahedra. The magnetic properties of V_4O_9 have been investigated by magnetic susceptibility, high-field magnetization and inelastic neutron scattering measurements. V_4O_9 is a spin-1/2 quantum spin system with a spin-gapped ground state. The excitation gap between the singlet ground state and the excited triplet state is approximately 73 K. The magnetic susceptibility behavior of V_4O_9 suggests that this compound is a spin-1/2 dimer system with significant interdimer interactions, as opposed to $(VO)_2P_2O_7$, which is an alternating spin-1/2 chain system. This difference is thought to be due to the fact that VO_4-mediated interactions are considerably weaker than PO_4-mediated interactions.

Acknowledgments

This work was supported in part by Global COE Program (Chemistry Innovation through Cooperation of Science and Engineering), MEXT, Japan and by a Grant-in-Aid for Scientific Research (No. 18104008) from the Japan Society for the Promotion of Science. One of the authors, YU, dedicates this study to the late Professor S. Kachi and the emeritus Professor K. Kosuge, University of Kyoto, Japan.

References

[1] N.F. Mott, Metal-Insulator Transitions, Taylor & Francis LTD, London, 1974.
[2] S. Kachi, K. Kosuge, H. Okinaka, J. Solid State Chem. 6 (1973) 258.
[3] F. Traina, M. Cucchett, A. Cappelli, A. Collina, M. Dente, Chim. L Industria 52 (1970) 329.
[4] S. Anderson, A. Sundholm, A. Magneli, Acta Chem. Scand. 13 (1959) 989.
[5] J.S. Anderson, B.G. Hyde, J. Phys. Chem. Solids 28 (1967) 1393.
[6] Y. Ueda, K. Kosuge, S. Kachi, Mater. Res. Bull. 12 (1977) 763.
[7] A.D. Wadsley, Acta Cryst. 10 (1957) 261.
[8] J. Tudo, G. Tridot, Compt. Rend. 261 (1965) 2911.
[9] K. Waltersson, B. Forslund, K.A. Wilhelmi, S. Andersson, J. Galey, Acta Cryst. B 30 (1974) 2644.
[10] K.A. Wilhelmi, K. Waltersson, L. Kihlborg, Acta Chem. Scad. 25 (1971) 1675.
[11] K. Kawashima, Y. Ueda, K. Kosuge, S. Kachi, J. Cryst. Growth 26 (1974) 321.
[12] Y. Ueda, K. Kosuge, S. Kachi, Mater. Res. Bull. 11 (1976) 293.
[13] A. Heidemann, K. Kosuge, Y. Ueda, S. Kachi, Phys. Status Solidi (a) 39 (1977) K37.
[14] H. Nishihara, Y. Ueda, K. Kosuge, H. Yasuoka, S. Kachi, J. Phys. Soc. Jpn. 47 (1979) 790.
[15] M. Taniguchi, A. Miyazaki, H. Yokomizo, Shokubai 10 (1968) 103 (in Japanese);
M. Taniguchi, S. Sato, T. Nanao, Shokubai 14 (1972) 53.
[16] K.A. Wilhelmi, K. Waltersson, Acta Chem. Scand. 24 (1970) 3409.
[17] K. Kawashima, K. Kosuge, S. Kachi, Chem. Lett. (1975) 1131.
[18] F. Théobald, R. Cabala, J. Bernard, Compt. Rend. C266 (1968) 1534; C269 (1969) 1209.
[19] F. Théobald, R. Cabala, J. Bernard, J. Solid State Chem. 17 (1976) 431.
[20] P.Y. Zavalij, M.S. Whittingham, Acta Cryst. B 55 (1999) 627.
[21] F. Izumi, T. Ikeda, Mater. Sci. Forum 321–324 (2000) 241.
[22] J.W. Johnson, D.C. Johnston, A.J. Jacobson, J.F. Brody, J. Am. Chem. Soc. 106 (1984) 8123;
D.C. Johnston, J.W. Johnson, D.B. Goshorn, A.J. Jacobson, Phys. Rev. B 35 (1987) 219.
[23] M. Azuma, T. Saito, Y. Fujishiro, Z. Hiroi, M. Takano, F. Izumi, T. Kamiyama, T. Ikeda, Y. Narumi, K. Kindo, Phys. Rev. B 60 (1999) 10145.
[24] M. Troyer, H. Tsunetsugu, D. Würtz, Phys. Rev. B 50 (1994) 1981.
[25] R. M. Contractor, H.E. Bergna, H.S. Horowitz, C.M. Blackstone, U. Chowdhry, A.W. Sleight, Catalysis 198, Elsevier, 645 (1988).
[26] P.T. Nguyen, R.D. Hoffman, A.W. Sleight, Mater. Res. Bull. 30 (1995) 1055;
Goto, H. Ohta, W. Utsumi, P. Bordet, D.C. Johnston, J. Solid State Chem. 153 (2000) 12.
[27] T. Saito, T. Terashima, M. Azuma, M. Takano, T. Goto, H. Ohta, W. Utsumi, P. Bordet, D.C. Johnston, J. Solid State Chem. 153 (2000) 124.
[28] A.W. Garret, S.E. Nagler, D.A. Tennant, B.C. Sales, T. Barnes, Phys. Rev. Lett. 793 (1997) 745.
[29] T. Yamauchi, Y. Narumi, J. Kikuchi, Y. Ueda, K. Tatani, T.C. Kobayashi, K. Kindo, K. Motoya, Phys. Rev. Lett. 83 (1999) 3729;
J. Kikuchi, K. Motoya, T. Yamauchi, Y. Ueda, Phys. Rev. B 60 (1999) 6731.
[30] J.C. Bonner, H.W.J. Blöte, J.W. Bray, S. Jacobs, J. Appl. Phys. 50 (1979) 1810;
J.C. Bonner, H.W.J. Blöte, Phys. Rev. B 25 (1982) 6959.
[31] D.C. Johnston, T. Saito, M. Azuma, M. Takano, T. Yamauchi, Y. Ueda, Phys. Rev. B 64 (2001) 134403.
[32] Y. Ueda, Chem. Mater. 10 (1998) 2653.
[33] H. Kageyama, K. Yoshimura, R. Stern, N.V. Mushnikov, K. Onizuka, M. Kato, K. Kosuge, C.P. Slichter, T. Goto, Y. Ueda, Phys. Rev. Lett. 82 (1999) 3168.